

## ACOUSTICS OF MARTIAN GEOLOGICAL MATERIAL FROM THE SHOCK WAVES OF THE LASER-INDUCED SPARKS OF SUPERCAM

C. Alvarez<sup>1</sup>, J. Laserna<sup>1</sup>, J. Moros<sup>1</sup>, P. Purohit<sup>1</sup>, S. M. Angel<sup>2</sup>, P. Bernardi<sup>3</sup>, O. Beyssac<sup>4</sup>, B. Bousquet<sup>5</sup>, A. Cadu<sup>6</sup>, B. Chide<sup>6,7</sup>, E. Clavé<sup>5</sup>, E. Dauson<sup>8</sup>, O. Forni<sup>7</sup>, T. Fouchet<sup>5</sup>, O. Gasnault<sup>7</sup>, X. Jacob<sup>9</sup>, G. Lacombe<sup>7</sup>, N.L. Lanza<sup>8</sup>, C. Larmat<sup>8</sup>, J. Lasue<sup>7</sup>, R.D. Lorenz<sup>10</sup>, P.-Y. Meslin<sup>7</sup>, D. Mimoun<sup>6</sup>, F. Montmessin<sup>11</sup>, N. Murdoch<sup>6</sup>, A. M. Ollila<sup>8</sup>, P. Pilleri<sup>7</sup>, A. L. Reyes-Newell<sup>8</sup>, S. Schröder<sup>12</sup>, A. Stott<sup>6</sup>, J. Ten Cate<sup>8</sup>, D. Vogt<sup>12</sup>, S. Clegg<sup>8</sup>, A. Cousin<sup>7</sup>, S. Maurice<sup>7</sup>, R. C. Wiens<sup>13</sup>, and the SuperCam Acoustics and LIBS Working Groups, <sup>1</sup>Departamento de Química Analítica, Universidad de Málaga, Málaga, Spain, <sup>2</sup>Department of Chemistry and Biochemistry, University of South Carolina, Columbia, SC, USA, <sup>3</sup>Laboratoire d'Etudes Spatiales et d'Instrumentation en Astrophysique, Observatoire de Paris-PSL, CNRS, Sorbonne Université, Université de Paris Cité, Meudon, France, <sup>4</sup>Institut de Minéralogie, de Physique des Matériaux et de Cosmochimie, CNRS, Sorbonne Université, Muséum National d'Histoire Naturelle, Paris, France, <sup>5</sup>Centre Lasers Intenses et Applications, CNRS, CEA, Université de Bordeaux, Bordeaux, France, <sup>6</sup>Institut Supérieur de l'Aéronautique et de l'Espace (ISAE-SUPAERO), Université de Toulouse, SAE-SUPAERO, Toulouse, France, <sup>7</sup>Institut de Recherche en Astrophysique et Planetologie (IRAP), Université de Toulouse 3 Paul Sabatier, UPS, CNRS, CNES, Toulouse, France RAP-CNRS, Toulouse, France, <sup>8</sup>Los Alamos National Laboratory, Los Alamos, NM, USA, <sup>9</sup>Institut de Mécanique des Fluides, Université de Toulouse 3 Paul Sabatier, Institut National Polytechnique de Toulouse, Toulouse, France Toulouse, France, <sup>10</sup>Johns Hopkins University Applied Physics Laboratory, Laurel, MD, USA, <sup>11</sup>Laboratoire Atmosphères, Milieux, Observations Spatiales, CNRS, Université Saint-Quentin-en-Yvelines, Université Paris Saclay, Sorbonne Université, Guyancourt, France Guyancourt, France, <sup>12</sup>Deutsches Zentrum für Luft- und Raumfahrt (DLR), Institute of Optical Sensor Systems, Berlin, Germany, <sup>13</sup>Earth, Atmospheric, and Planetary Sciences, Purdue University, West Lafayette, IN, USA

**Introduction:** SuperCam is a remote-sensing instrument onboard the rover Perseverance for the Mars 2020 mission that uses multiple analytical techniques (LIBS, Raman, time-resolved fluorescence and visible and near infrared reflectance spectroscopy) for remote spectral measurements to determine fine-scale mineralogy, chemistry, and atomic and molecular composition of Mars geological materials at the Jezero crater. In addition, SuperCam also performs acoustics studies on how sound is transmitted in the Mars' thin atmosphere, on events as wind and turbulence, and on the sound of the laser-induced plasma shock waves from geological targets. SuperCam's microphone records pressure fluctuations from 20 Hz to 50 kHz, at a sampling rate of 100 kHz. The microphone is synchronized to the laser pulses, recording a time of 60 ms around the laser shot (the laser repetition rate is 3 Hz, so there is a data gap between two consecutive shots). The microphone recorded laser-induced shock waves up to 9.2 m.<sup>1,2</sup>

**Samples:** Research focuses on the targets interrogated during the first 380 Sols on Mars from the Perseverance landing, during which the rover traversed two geological formations labelled as "Máaz" and "Séítah" in Jezero crater. Significant chemical differences were identified from

SuperCam spectral measurements. Furthermore, within Séítah, a group of pitted, less crystalline rocks comprise the "Content member", and variably recessive and massive outcrops below and on top of a ridge nicknamed "Artuby" were labeled.<sup>3,4</sup>

Within them, results from 4 types of targets are reported by simultaneous LIBS and acoustic measurements:

- Bulk rocks (76% of the acoustic analyzed targets). Rocks with a size significantly larger than the laser-matter interaction area.
- Abraded patches (11%). Rock surfaces abraded by the rover during the studies related to collecting samples for a future send-back to Earth.
- Regolith (11%). Soil and soil with granular sub-millimeter grains close to the diameter of the laser spot (300 – 600 μm).
- Drill tailings (2%). Pulverized targets generated during the drilling process with minimal compaction.

From all them, a total of 234 different targets were observed, each interrogated at 5, 9, or (mostly) 10 positions on the surface.

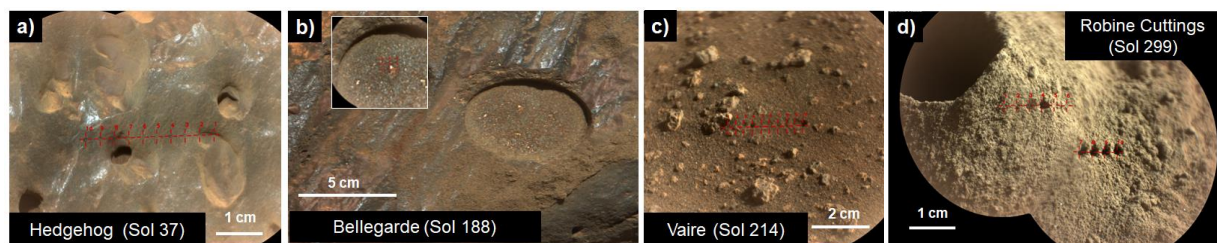


Fig. 1. Images of examples for a) bulk rock; b) abraded patches; c) regolith; and d) drill tailings targets. The black labels provide the target name and the sol number for the analysis. The crosses in red identify the LIBS sampling positions.

## Results and discussion:

**Comparing geological targets.** Different measurements were considered to compare the four geological populations: the peak-to-peak amplitude of the first compression-rarefaction in the impedance corrected-acoustic wave and the total emission of the LIBS spectra as analytical signals, their corresponding relative standard deviation (RSD) to track the variability of data and its evolution within homologously-catalogued targets, and the signal decay to track the variation of the signal intensity for a series of laser pulses performed at the same analysis position.

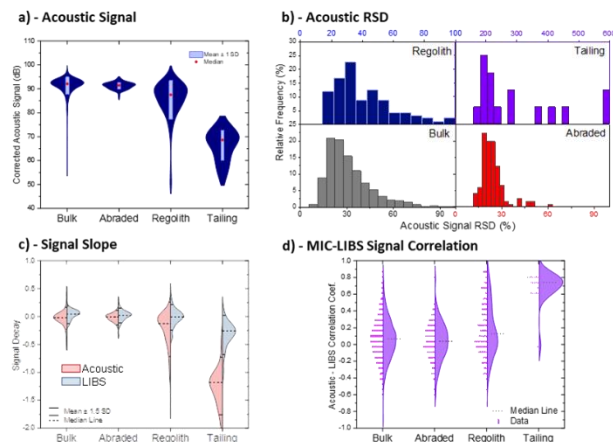


Fig. 2. a) Acoustic signal violin and box plots (red point is the median). b) Histogram for the intra-position RSD (%). c) Variation of the averaged acoustic and LIBS slope per target population. (d) Distribution of the correlation values between simultaneous MIC-LIBS analytical signals from sparks of targets conforming each population.

Figure 2a displays violin plots showing the relationship of the corrected acoustic signal to the type of target and Figure 2b presents the histograms showing how frequently the intra-position relative standard deviation of the acoustic signals falls into a particular bin. Data reveals that laser-driven acoustics for targets with a granular or less cohesive structure (regolith and tailings) significantly differs from that of bulk and abraded patches, considered as "consolidated surfaces", either in intensity (a lower amplitude in the case of tailing targets) or in stability (a broad range of amplitudes in the case of regolith). At the same time, it should be noted how the most powdered targets/less compacted, that is from "tailing" population, for which the acoustic intensity decays more noticeably within a singular sampling point (Figure 2c), the highest correlation is observed between acoustic and optical emission from sparks (Figure 2d).

**Comparing geological units.** Acoustic signals related to the geological units "Séítah" and "Mááz" were analyzed focusing on "bulk" and "abraded"

populations given their lower variability. Figure 3 compares the acoustic signals generated from the different targets grouped according to their inferred pyroxene and olivine compositions from the mineral stoichiometry derived from LIBS measurements. It must be noted that while Séítah is dominated by olivine, confirmed by all three SuperCam spectral techniques, pyroxenes were identified in both the Séítah and Mááz formations.

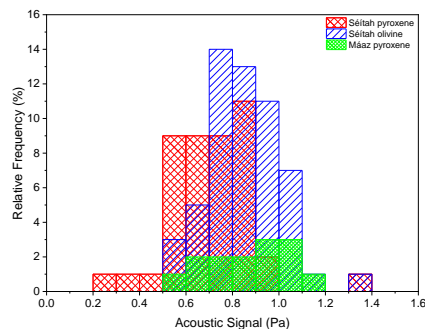


Fig. 3. Distribution of the acoustic signal for the pyroxene and olivine targets found at the Séítah and Mááz geological units during the Perseverance path through Jezero crater floor.

As seen, within Séítah, the median acoustic signal from olivine targets appears to be slightly higher than that from pyroxenes. This could be argued by the slightly higher densities of olivines, inferred from their larger molar ( $Mg+Fe$ ) since they contain less Si. At the same time, the Fe/Mg ratio, almost constant in the case of olivines but much more variable for pyroxenes, could justify the skewed distribution of pyroxene acoustic responses. Indeed, when pyroxenes identified in "Séítah" and "Mááz" are compared, both reveal a parallel skewed distribution, although "Mááz" pyroxenes show slightly higher acoustic signals. These results fit with the differences identified between "Mááz" and "Séítah" in terms of mineral stoichiometry derived from LIBS, particularly for the compositions inferred for their pyroxenes.<sup>5,6</sup>

**Acknowledgments:** Research funded by projects UMA18-FEDERJA-272 from Junta de Andalucía and PID2020-119185GB-I00 from Ministerio de Ciencia e Innovación, of Spain. P.P. is grateful to the European Union's NGEU plan and the Spanish Ministerio de Universidades for his Margarita Salas fellowship under the program "Ayudas para la Recualificación del Sistema Universitario Español".

**References:** [1] Wiens, R.C. *et al. Space Sci. Rev.*, 217, 4 (2021). [2] Maurice, S. *et al. Space Sci. Rev.*, 217, 47 (2021). [3] Farley, K.A. *et al. Science*, 377, (2022). [4] Wiens, R.C. *et al. Sci. Adv.*, 8, (2022). [5] Udry, A. *et al. J. Geophys. Res. Planets*, 127, (2022). [6] Liu, Y. *et al. Science* 377, (2022).